NASA/CR-2007-214885/VOL1

Hypervelocity Impact (HVI)

Volume 1: General Introduction

Michael R. Gorman and Steven M. Ziola
Digital Wave Corporation, Englewood, Colorado

September 2007

The NASA STI Program Office . . . in Profile

Since its founding, NASA has been dedicated to the advancement of aeronautics and space science. The NASA Scientific and Technical Information (STI) Program Office plays a key part in helping NASA maintain this important role.

The NASA STI Program Office is operated by Langley Research Center, the lead center for NASA's scientific and technical information. The NASA STI Program Office provides access to the NASA STI Database, the largest collection of aeronautical and space science STI in the world. The Program Office is also NASA's institutional mechanism for disseminating the results of its research and development activities. These results are published by NASA in the NASA STI Report Series, which includes the following report types:

- TECHNICAL PUBLICATION. Reports of completed research or a major significant phase of research that present the results of NASA programs and include extensive data or theoretical analysis. Includes compilations of significant scientific and technical data and information deemed to be of continuing reference value. NASA counterpart of peer-reviewed formal professional papers, but having less stringent limitations on manuscript length and extent of graphic presentations.

- TECHNICAL MEMORANDUM. Scientific and technical findings that are preliminary or of specialized interest, e.g., quick release reports, working papers, and bibliographies that contain minimal annotation. Does not contain extensive analysis.

- CONTRACTOR REPORT. Scientific and technical findings by NASA-sponsored contractors and grantees.

- CONFERENCE PUBLICATION. Collected papers from scientific and technical conferences, symposia, seminars, or other meetings sponsored or co-sponsored by NASA.

- SPECIAL PUBLICATION. Scientific, technical, or historical information from NASA programs, projects, and missions, often concerned with subjects having substantial public interest.

- TECHNICAL TRANSLATION. English-language translations of foreign scientific and technical material pertinent to NASA's mission.

Specialized services that complement the STI Program Office's diverse offerings include creating custom thesauri, building customized databases, organizing and publishing research results ... even providing videos.

For more information about the NASA STI Program Office, see the following:

- Access the NASA STI Program Home Page at ***http://www.sti.nasa.gov***

- E-mail your question via the Internet to help@sti.nasa.gov

- Fax your question to the NASA STI Help Desk at (301) 621-0134

- Phone the NASA STI Help Desk at (301) 621-0390

- Write to:
  NASA STI Help Desk
  NASA Center for AeroSpace Information
  7115 Standard Drive
  Hanover, MD 21076-1320

NASA/CR-2007-214885/VOL1

Hypervelocity Impact (HVI)

Volume 1: General Introduction

Michael R. Gorman and Steven M. Ziola
Digital Wave Corporation, Englewood, Colorado

National Aeronautics and
Space Administration

Langley Research Center
Hampton, Virginia 23681-2199

Prepared for Langley Research Center
under Contract NNL05AC19T

September 2007

Available from:

NASA Center for AeroSpace Information (CASI)
7115 Standard Drive
Hanover, MD 21076-1320
(301) 621-0390

National Technical Information Service (NTIS)
5285 Port Royal Road
Springfield, VA 22161-2171
(703) 605-6000

Hypervelocity Impact (HVI)
Volume 1: General Introduction

During 2003 and 2004, the Johnson Space Center's White Sands Testing Facility in Las Cruces, New Mexico conducted hypervelocity impact tests on the space shuttle wing leading edge.

Hypervelocity impact tests were conducted to determine if Micro-Meteoroid/Orbital Debris impacts could be reliably detected and located using simple passive ultrasonic methods.

This section contains an executive summary, overview of the method, brief descriptions of all targets, and highlights of results and conclusions.

Detailed reports for each target follow the General Introduction.

Table of Contents

List of Figures

Hypervelocity Impact (HVI)
Volume 1: General Introduction

Introduction

In the wake of the Columbia accident, NASA personnel decided to test the idea that impacts during space flight could be detected by acoustical sensors at ultrasonic frequencies. The substance of this idea rested on the knowledge that in laboratory experiments lower velocity impacts had created signals with frequencies in the 20 – 200 kHz range. If Shuttle engine and aerodynamic noise were down in the sonic range then locating impacts would be easier in the 20-200 kHz range. The questions were what frequencies would be created during hypervelocity impacts by tiny objects, would the ultrasonic energy be detectable and interpretable, and what would be the best way to detect impact and size the damage, keeping in mind the potential need for lightweight, simple installation procedures and low electrical energy consumption.

A further basis for selecting this method was that recent fundamental research had elucidated the basic physics of the ultrasonic signals created by the impacts in a variety of aerospace materials and geometries. This made it more likely that signal and noise could be separated and that subsequent analysis of the signals would yield the desired information about impact severity and location. All of the above reasoning proved to be correct. Hypervelocity impact by tiny aluminum spheres created signals in the 20-200 kHz frequency range easily detectable with small piezoelectric sensors similar to equipment being flown.

A summary of the relevant results, advantages and requirements of using ultrasonic sensors for impact detection are shown in bullet format below.

- **Advantages**
  - The method works during launch
  - Engine and other mechanical vibration noise sources are at lower frequencies which means lower background noise level in ultrasonic frequency range
  - Gives approximate size of damage
  - Resulting higher signal/noise ratio can make noise discrimination and impact detection easier
  - Provides damage location
  - Higher frequency provides increased location accuracy
  - Rugged, lightweight

- **Requirements Impact**
  - Recording higher frequencies requires more memory and higher sampling rate than currently on shuttle. This may impact battery life on wireless data acquisition systems.

- **Scientific Highlights**
  - Frequencies from 0 – 150 kHz were created
  - Filtering frequencies below 30 kHz did not affect analysis
  - Damage location calculable
  - Good correlation between damage size and acoustic energy
  - Explanation of relationship between supersonic source and plate waves.

- **Practical Results**
  - Sensor system functional in near vacuum
  - Sensors easily bonded to targets
  - System requirements similar to current flight instrumentation parameters
  - Data analysis straightforward

Targets

The number of targets tested in the overall HVI study was extensive as shown in the list below:

- A-1 – Fiberglass plate and aluminum plate with standoff rods (with grommets)
- A-2 – Fiberglass plate and aluminum plate with standoff rods (no grommets)
- B-1 –Two fiberglass plates and aluminum plate with standoff rods
- C-1 – Fiberglass flat plate
- C-2 – Fiberglass flat plate
- Fg(RCC)-1 – Fiberglass in the shape of Wing Leading Edge
- Fg(RCC)-2 – Fiberglass in the shape of Wing Leading Edge
- RCC16R – Carbon-Carbon Actual WLE
- A-1 Tile – Tile structure of forward part of wing with no gap filler
- Ag-1 Tile – Tile structure of forward part of wing with gap filler
- B-1 Tile – Tile structure of aft part of wing with no gap filler
- Bg-1 Tile – Tile structure of aft part of wing with gap filler

Each of the target reports features tables of kinetic energy and damage results, and a discussion of the linear relationship between kinetic energy, ultrasonic wave signal energy and damage. Also discussed are wave propagation effects, the wave modes and their velocities, and location of impacts by analysis of wave arrival times. The Appendix for each section has test condition data sheets, impact waveforms, and photos of the

damage for each shot. Also included are tables of impact data, gain settings, recorded wave signals, and damage results.

This section contains the overall goals, the personnel involved, the test methods, instrumentation, calibration, and overall results and conclusions.

Goals

Major questions answered in this program were:

- What frequencies are created by hypervelocity impact?
- What is the geometric area of structure that a single sensor can cover and with what location accuracy and damage assessment capability?
- Would the method work in a space vehicle's complex structural geometries?

Ultrasonic Data Archives

There exists a complete archive of all ultrasonic (AE) data files from impacts (foam, ice, ablator, hypervelocity, and impact hammer/UT tests) at NASA Langley Research Center.

Personnel Involved

Mr. George Studor, JSC, provided program direction. Dr. William Prosser, LaRC, was the lead investigator. Dr. Eric Madaras, LaRC, and Dr. Michael Gorman, Digital Wave Corporation, provided support in testing and data analysis.

Overview of Ultrasonic Method

Impacts create ultrasonic waves that can be detected by transducers and the source identified and located similarly to earthquakes and SONAR. The ultrasound method is called modal acoustic emission. This method was explored because it detects sound in a frequency range that should be acoustically quiet during all standard vehicle operations. The spectrum in this frequency range is unknown until flight testing takes place. However, from experience with jet aircraft testing it is reasonable to expect that most of the sound and vibration present, even during ascent, has most of its significant spectral content below 20 kHz.

Modal Acoustic Emission (MAE) analysis is based on the type of wave modes that propagate in engineering structures. The approach is similar to that of seismology and geophysics, where primary waves (p-waves) and secondary waves (s-waves) are analyzed to determine the source type, magnitude and location of earthquakes and impacts on the earth. P and S waves are bulk waves. Bulk waves propagate in unbounded media where the wavelength is very short compared to the dimensions of the medium. In structures built of plate-like sections (for example, aircraft wings, fuselages, etc.) the wave modes of interest are the extensional mode (in-plane stretching and compressing of the plate) and the flexural mode (bending of the plate). These are called plate waves. Plate waves

propagate in bounded media where the wavelength is larger than the thickness. Sometimes plate waves are referred to as guided waves since the waves are confined between the two surfaces of the plate as they propagate outward from the source.

Data Acquisition System

The tests were conducted on the 0.50 caliber hypervelocity launcher range at the White Sands Test Facility (WSTF). The flight range for the hypervelocity projectile and target chamber were evacuated to near vacuum pressure (6-8 Torr) prior to each shot. The AE recording equipment was connected by feed-throughs to the sensors on the target inside the vacuum chamber. The connectors were BNC type.

The projectiles were small spheres made of 2017 T-4 aluminum. They ranged in diameter from 0.4 mm to 6 mm. Impact velocity was measured with WSTF diagnostic equipment on each shot. Nominal velocity was 6.8 km/s.

Signals were detected with Digital Wave B225.5 sensors. The frequency response was flat from 60 kHz to 180 kHz, however there was still some response down to DC. There were high pass filters in the recording unit that rolled off at 20 kHz so signals that contained frequencies less than 20 kHz in reality contained quite a bit of energy since the sensors were rolling off towards the lower frequencies as well. Sensors were attached to the targets with Lord 202 fast cure acrylic adhesive.

After detection at the sensor, the signals passed through preamplifiers then filters and amplifiers. From there the signals went directly to an A/D card residing in the computer where they were digitized and stored on a hard drive during testing. The equipment is shown in

Figure 1. Digital Wave's Wave Explorer software handled acquisition and storage. It also displayed the captured waveforms live during the test.

The digitizer was capable of various sampling rates. Impact signals were digitized at 500 kHz sampling rate with 32 k samples for a total waveform window of 64 milliseconds. This time allowed enough pre-trigger time for a clean front end before the impact and enough post-trigger time for the reverberations to die out.

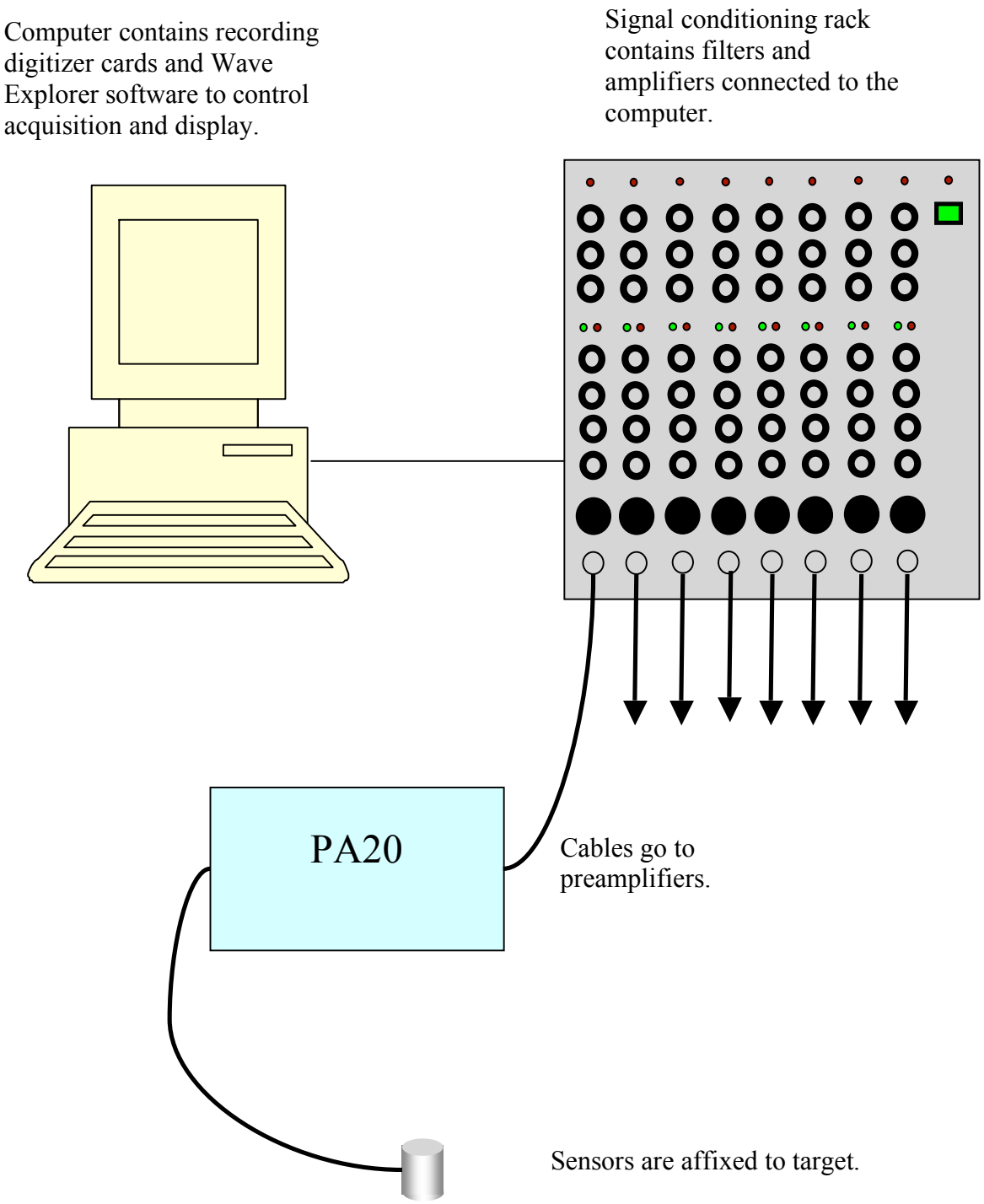

Figure 1: Modal AE Recording Equipment.

Sensor Calibration

The two calibration methods used were a primary NIST calibration method and a secondary calibration against NIST standard reference sensors. The primary method simulated an acoustic emission (AE) source on large steel calibration block and utilized an absolutely calibrated Michelson interferometer detector. The sensor was placed a distance of 5 cm away from the center on the polished surface of a cylindrical block of steel (large compared to wavelength of sound) and acoustically coupled to the block with vacuum grease. Another transducer was placed at the center of the face. This was used to provide the source pulse. An absolute Michelson laser interferometer was focused at a point the same distance from the center and on the line connecting the center point with the sensor under test. Thus this was a symmetrical arrangement and since the sound propagates symmetrically outward in all directions the displacement measured by laser can be compared to the voltage measured by the sensor being calibrated. The resulting absolute calibration curve is shown in Figure 2.

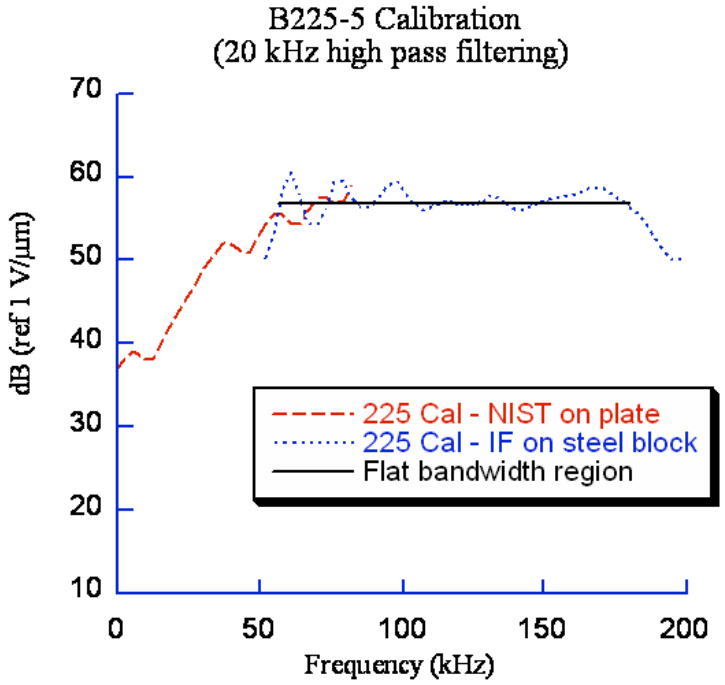

Figure 2: Calibration Curve for B225-5 AE Sensor
Based on Rayleigh surface wave propagating on large steel block.
Measured with Michelson interferometer.

The response was flat from 60 to 180 kHz with 57 dB (708 V/mm) calibration factor. Sensor only calibration (without 20 kHz high pass filtering) levels off at 45 dB at low frequencies. Smaller lateral dimensions limit low frequency calibration.

The secondary method simulated an AE source on large aluminum plate with an absolutely calibrated NIST conical standard reference sensor. This method allows calibration to lower frequencies, but limited at higher frequencies

Calibration of In-Line Attenuators

For many of the large impacts, attenuation was necessary to prevent saturation of the preamplifiers. Depending on the size of the impact signal, the measurement conditions consisted of either no in-line attenuators, a 10 dB attenuator, a 20 dB attenuator, or 10 and 20 dB attenuators in series. The preamp and system gain was varied to boost signal to acceptable levels. The attenuators were calibrated with a tone burst input signal driving DWC 225 sensor face-to-face against DWC 225 receiving sensor. The input amplitude held constant while the frequency was varied (30, 40, 60, 80 and 100 kHz). Peak signal amplitude was measured near center of toneburst. The calculated attenuation was relative to no attenuator condition.

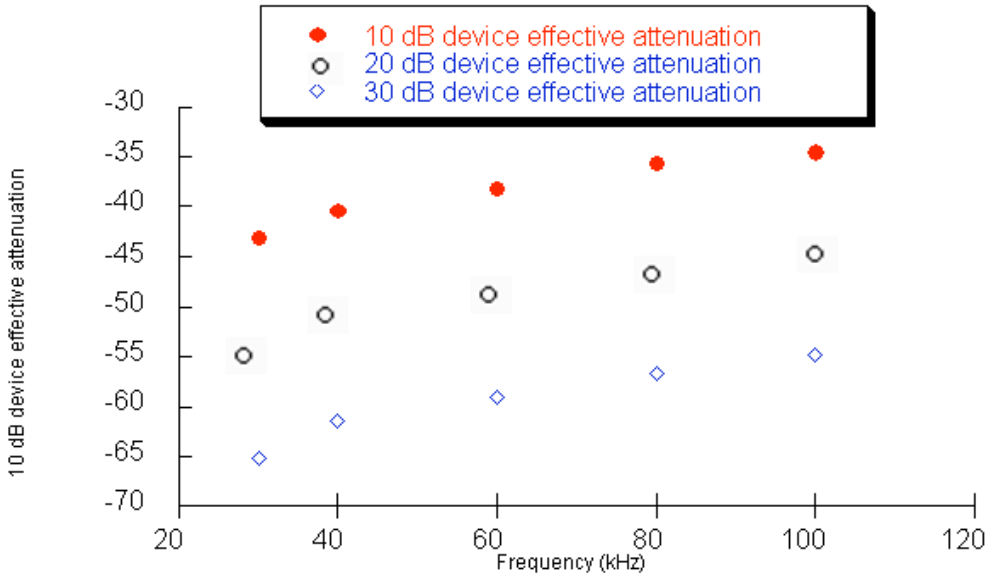

Figure 3: Device Effective Attenuation

The frequency dependence of attenuation observed (Figure 3) increased more significantly below 40 kHz, but could not drive transducers very well below 30 kHz. These were intended as 50 Ohm attenuators but were connected to the preamp that had a 10 kOhm input impedance so they did not simply attenuate to the value stamped on them. A 6 dB attenuator produced about 40 dB attenuation due to the impedance mismatch. These were the only attenuators available at the time. The previous value determined for 30 dB (10 and 20 dB attenuators in series) was ~50 dB based on peak amplitude measurements for a broad band (lead break input source). The narrowband tone burst

value was ~55 dB at 100 kHz. The difference is attributable to higher frequency content in broadband calibration measurement

Data Analysis

Defect growth (e.g., a crack) in plates shows certain characteristics related to the source motion. The source motion is the displacement of the crack faces. The motion is usually perpendicular to the normal to the plate. The wave motion follows from the source motion. Thus a crack creates a propagating extensional mode. Due to Poisson action some out-of-plane motion is also present. This is how a sensor on the surface detects the presence of the E wave. Sources such as corrosion and rust on the plate surface create a source motion perpendicular to the plane of the plate and cause the plate to bend (much like striking the head of a drum) as the wave propagates. These sources create large flexural modes. The E and F modes have very distinct characteristics (see Figure 4 or Figure 5 below), and can be identified.

It can be seen that the lower frequencies arrive before the higher frequencies in the first example (Figure 4) which is extensional mode created by breaking a mechanical pencil lead against the edge of an aluminum plate. The second example (Figure 5) shows a small extensional wave at the front followed by a large flexural wave. This example was created by breaking a pencil lead on the surface of the plate. It can be readily seen that the lower frequencies arrive later than the flexural mode, just the opposite of the behavior of the extensional mode. If these were observed at a later time, the sinusoidal components would be spread further apart. The most important point here is that there is an intimate connection to the source motion. Out of plane sources produce flexural waves and in plane sources produce extensional waves.

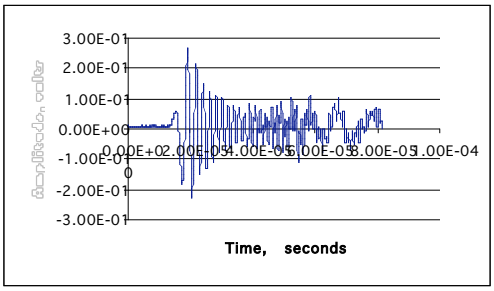

Figure 4: Large Extensional Wave Followed by Small Flexural Wave

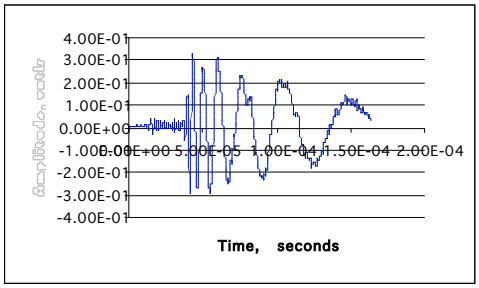

Figure 5: Small Extensional Wave Followed by Large Flexural Wave

The physics of MAE is similar to that of vibrations. A pulse can be considered as the sum of sinusoidal (Fourier) frequencies, each frequency representing a certain mode of vibration. The term mode means shape of the motion. For example, the back and forth motion of a violin string consists of several individual modes called the fundamental and its harmonics. In the case of the string the mode shapes are sinusoids. In plates, the Fourier frequencies in a pulse move (propagate) at different speeds, so the pulse disperses (changes shape) as it propagates.

At the frequencies of the acoustic emission of interest here (20-200 kHz), the waves have definite mode shapes. Essentially the waves consist of vibrations at higher frequencies than normally associated with structural vibrations so that the motion appears localized at any given moment in time instead of spread over the entire medium. Waves are often called ‘disturbances’ in the ‘medium’ that propagate through the medium (the structure). A disturbance transits from one part of the medium to the other and then ‘reflects’ back from the edge and ‘interferes’ with itself and/or other reflections.

An impact event creates a transient in the medium that can be analyzed using Fourier analysis. Fourier analysis states that any shape transient can be considered as the sum of sines and cosines. The sines and cosines add together in such a way as to produce distinctive particle motions that move with time through the material. Wave modes are slightly more complicated to visualize than low frequency vibrational modes in that each wave ‘mode’ contains many sinusoidal components rather than a single frequency. Different sources excite the wave modes differently which makes it is possible to distinguish sources.

By analyzing mode shapes, and taking into account the material and loading, sources can be identified and located. The direct connection to fundamental physics is a key characteristic of MAE. For simple geometries the wave shapes and velocities have been calculated from wave equations derived from Newton’s laws of motion and they compare well with measurements. By using arrival times at transducers with known positions, the location of the source can be triangulated by various mathematical methods (similar to methods used in SONAR).

Hypervelocity impact (HVI) events create both flexural and extensional types of waves depending on the target and the degree of damage. It is these waves that were detected and analyzed under this program. Sound reverberates throughout most media, but fiberglass damps sound much more rapidly than aluminum. Usually, reflections take a

tens of milliseconds or longer to die out. Complex structures have many reflection points that can add a lot of distortion, so the first part of the signal, called the direct wave, is sought and is the subject of most of the analysis. Analysis consists of identifying the source, locating the source and assessing the intensity of the source so that something about the level of damage may be inferred.

The inhomogeneities in the propagation path create distortion because the different frequency components interfere with each other as they pass around an obstacle and recombine on the other side. A sensor coupled to a leading edge wing spar receives the sound only indirectly. The sound propagates from the impact position through all the connection points and then into the spar. The sound echoes in all the pins and these echoes interfere. This makes identifying the modes difficult.

The piezoelectric sensors converted the sound wave energy to electrical voltages. The energy computed from the voltage data collected by each sensor channel is referred to as the wave signal energy. The wave signal energy for each channel was analyzed and compared to the impact energy. The wave signal energy was computed by integrating the squared voltage, V, with respect to time and dividing this number by the impedance at the preamp input, R (Equation 1).

$$E_{raw} = \frac{1}{R}\int V^2 dt \qquad \textbf{Equation 1}$$

The voltage versus time values of the wave, which were displayed in the waveform window on the computer screen for each channel, were not corrected for any applied gain (or attenuation). Attenuation was the norm because hypervelocity impact produced very energetic signals that in most cases would have saturated the A/D converter on the recording card in the computer had the amplitude not been reduced.

The MAE software computed the raw wave signal energy in Joules uncorrected for any analog gain or attenuation that may have been applied to the signal path. In order to compare the wave energies from shot to shot, the raw wave signal energy was converted by applying Equation 2 where E_{raw} is the energy computed using the recorded wave (with DC offset eliminated) and G is the system gain.

$$W.S.E. = \frac{E_{raw}}{G^2} \qquad \textbf{Equation 2}$$

The gain G was computed by converting the logarithmic gain, M, in decibels with Equation 3 or Equation 4.

$$M\ dB = 20\ Log_{10}\ (G) \qquad \textbf{Equation 3}$$

$$G = 10^{\frac{M}{20}}$$ **Equation 4**

The wave signal energy collected by sensor on the surface of all targets was on the order of 10^{-4} Joules. Sensors located on the spar for Targets Fg(RCC)-1, Fg(RCC)-2, and RCC16R collected recorded wave signal energy on the order of nanoJoules. For consistency, wave signal energy is always expressed in nJ throughout the Report.

Location Analysis

Sensors were placed in such way as to surround the intended impact positions for each target. The sensor array was square on the simple plates. A square array makes source location easier and more accurate.

Source location analysis is based on triangulation of the source based on the arrival times at each sensor and the appropriate wave velocities. The arrival time was determined by placing a cursor at the first cycle of the extensional wave in each of the waveform windows. This was the earliest arriving portion of the direct wave. The software that displays the captured signals also displays the time at the position of the cursor. Since each waveform was digitized at the same sampling rate, the time differences or delta times give the absolute differences in arrival times in microseconds.

A detailed example of location analysis is given in Target Fg(RCC)-1.

Frequency Influence

The raw wave signal energy was processed by removing low frequency noise with WaveExplorer software. Filtering low frequency noise did not affect the arrival time for ultrasonic sensors. For example, see RCC16R impacts #16 and #20 (Figure 6 - Figure 9). Frequencies under 50 kHz were eliminated using a digital highpass filter without affecting the recorded arrival times. The importance of arrival times is discussed in Location Analysis.

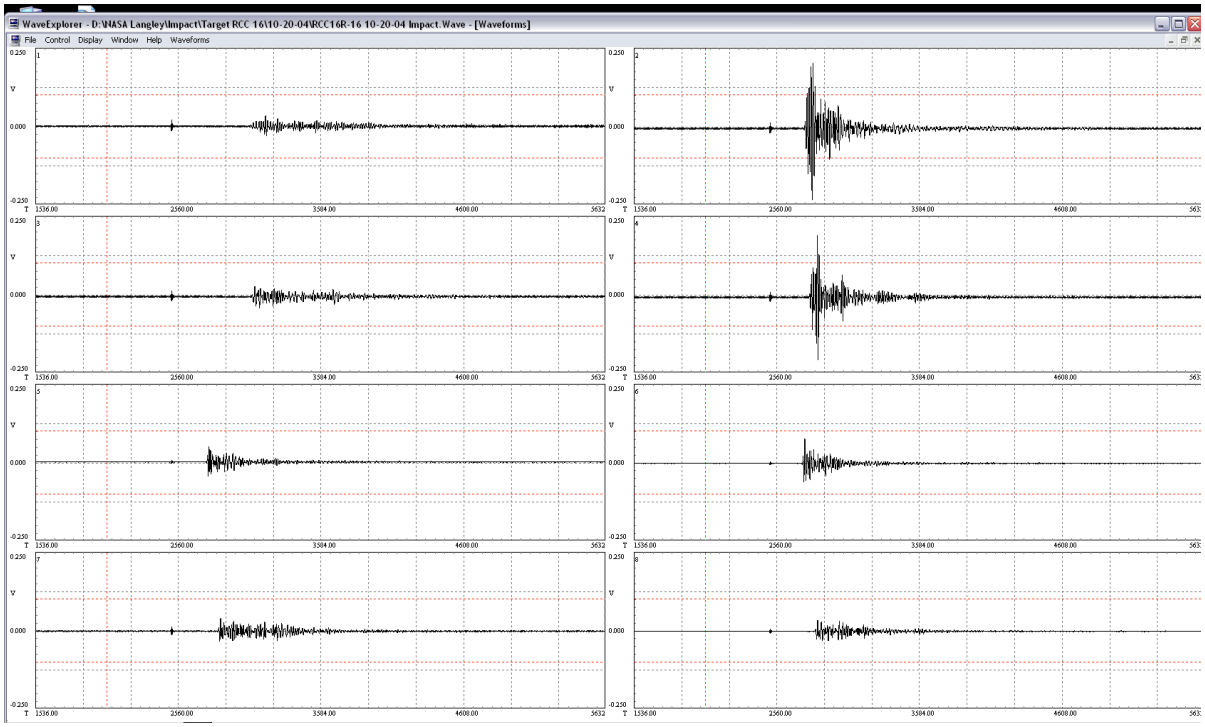

Figure 6: RCC16R Shot #16 Impact Waveform – Unfiltered

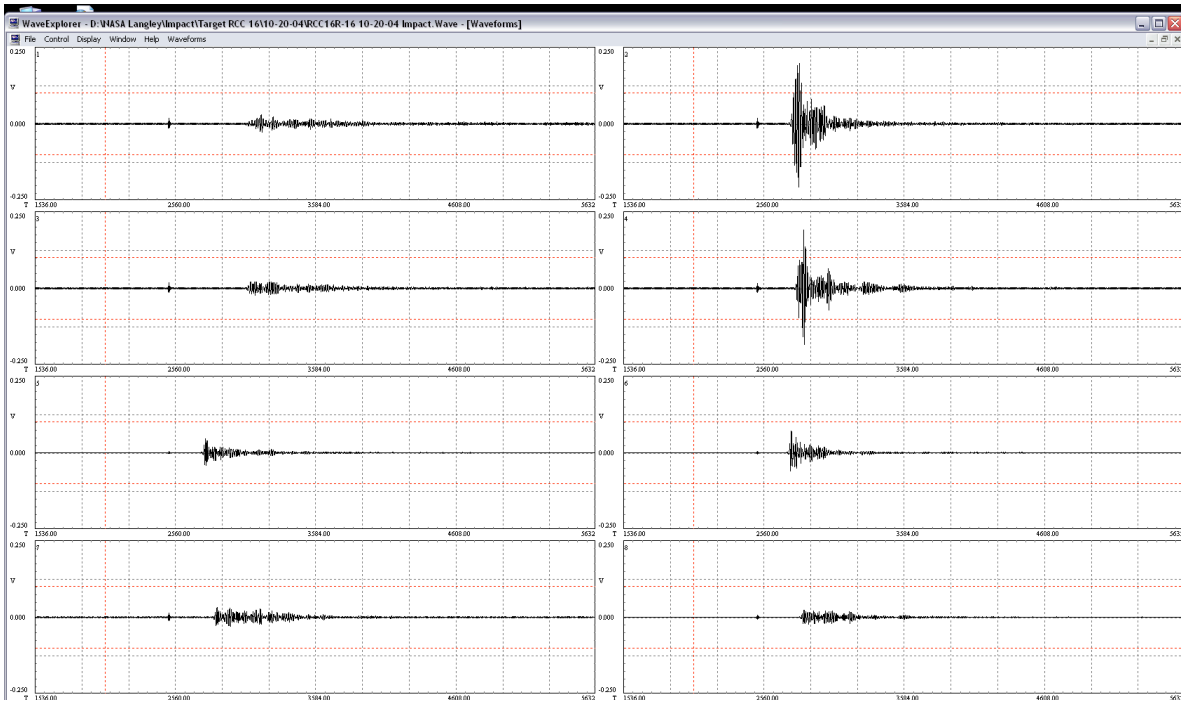

Figure 7: RCC16R Shot #16 Impact Waveform - 50 kHz Highpass Filter

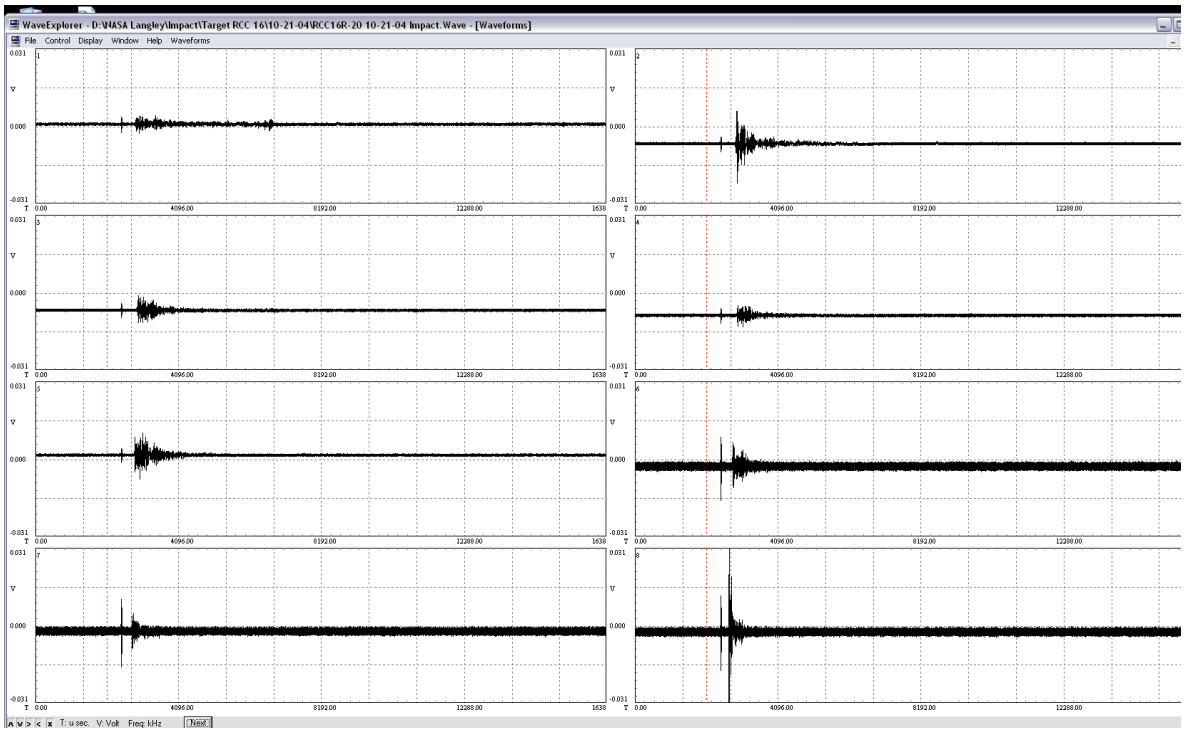

Figure 8: RCC16R Shot #20 Impact Waveform – Unfiltered

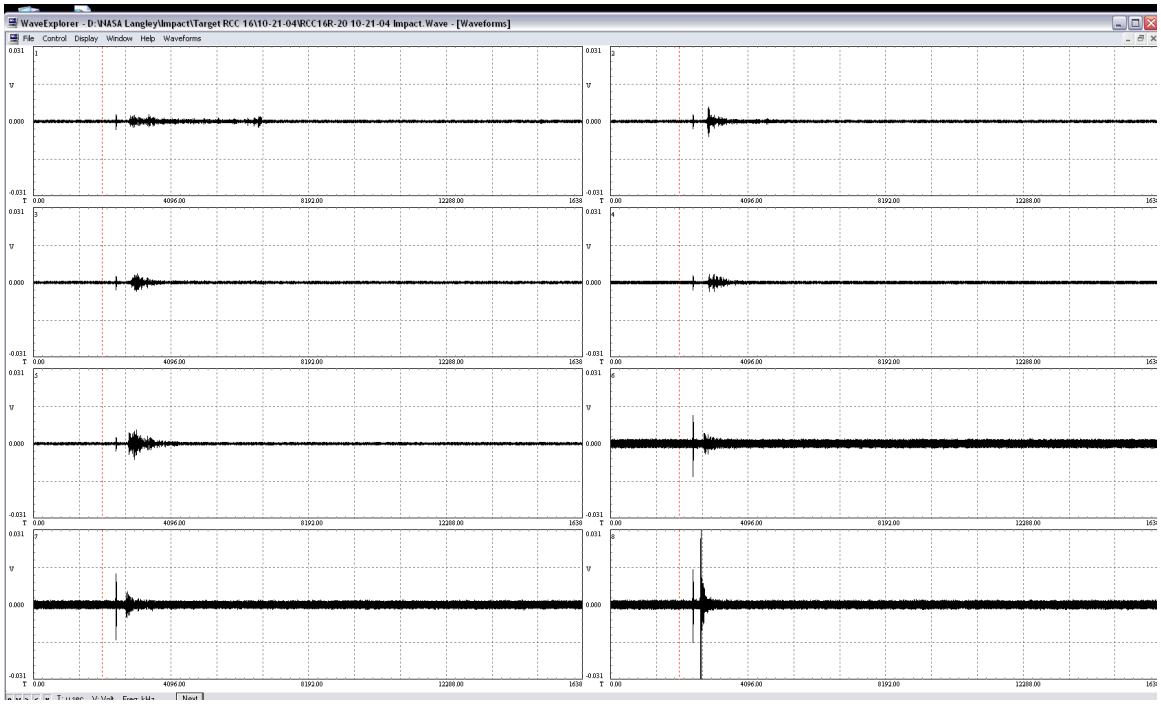

Figure 9: RCC16R Shot #20 Impact Waveform - 50 kHz Highpass Filter

Effects of Fast Moving Sources in Wave Mode Development

The impactor was moving at nearly 7 km/s but the velocity of sound in the E mode is about 4 km/s and the velocity of sound in the F mode is only about 2 km/s. This means that the impactor is supersonic in the material and thus a shock wave is formed. The motion of the shock wave is a conical and nearly in plane source motion is achieved. Thus for the higher kinetic energies where complete penetration is achieved the motion of the disturbance is in the plane of the plate which is why the disturbance propagates predominantly as the E mode.

Another way to look at the forcing function of the disturbance is to consider how long a time it takes the impactor to traverse the target thickness. Considering a 90 deg shot and a target thickness of 6 mm, it takes less than a microsecond. The sound waves do not propagate this fast so they are just beginning to form in this short time. For the even slower F mode there is no time to form. The effect is essentially the nearly instantaneous application of a dipole forcing function in the plane of the plate that creates an E wave.

If the material liquefies during impact, the effect would be emphasized due to the even slower velocity of sound in a liquid compared to a solid.

On the other hand, as the impactor slows to subsonic during crater formation, an F mode would be possible. In the case of a crater, the F mode formation depends on several factors including the angle of impact, diameter of the impactor, impactor material, and the kinetic energy. In principle it should be possible to determine the depth of the crater from these parameters and, since these factors determine the relative energies in the modes, crater depth can in principle be determined by the sound waves created. It is known that impactors disintegrate and there are all kinds of ejecta as well

The above hypotheses are confirmed by close examination of the recorded sound waves. The E mode and F mode are identifiable in the data. The F wave travels more slowly so the E and F begin to separate as the disturbance propagates toward distant sensors. The relative energies in the two modes result from the source motion but are modified by the propagation characteristics of the medium. In the case of complete penetration where a hole is left in the material the disturbance propagates mainly as an E mode. When impactor either comes to rest or ricochets off the target, a crater is formed and the disturbance propagates with energy in both the E and F modes.

This means that detectors installed on critical components of spacecraft could indicate penetration or lack of penetration. Space Shuttle windows come to mind as a particularly straightforward application. The main requirement from an acoustical point of view is a homogeneous propagation path so the modes can be identified.

Kinetic Energy and Wave Signal Energy

For design engineering and threat analysis purposes, shots were performed at various angles to the normal to the target at the point of impact. It was suggested by Summers

(NASA TN D-94, 1959) that only the normal kinetic energy be used to compare with crater depth. Figure 10 shows a simulation of an angled hypervelocity impact. It is evident that not all of the kinetic energy is in the normal direction. For comparison, both the total kinetic energy and the kinetic energy for the normal velocity component was computed (sine squared of the angle, ninety degrees is normal). Normal KE is just the kinetic energy associated with the projectile velocity component normal to the target surface at the point of impact. Uncertainty calculations for total and normal kinetic energy are given in the Appendix to this section.

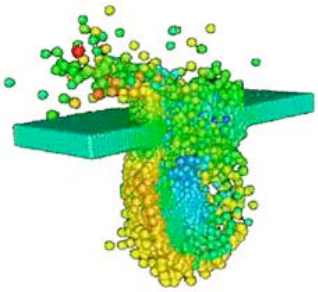

Figure 10: Simulation of Angled Hypervelocity Impact[1]

Relative Uncertainty of Total Kinetic Energy

d = diameter, m
ρ = density, kg/m^3
v = velocity, m/s
Δd = diameter uncertainty, m
Δv = velocity uncertainty, m/s

$$K.E. = \frac{1}{2}\left[\frac{4}{3}\pi\left(\frac{d}{2}\right)^3\rho\right]\left[v\right]^2$$

$$K.E. + \Delta K.E. = \frac{\pi\rho}{12}\left(d+\Delta d\right)^3\left(v+\Delta v\right)^2$$

Expand.

$$= \frac{\pi\rho}{12}\left(\begin{array}{l} v^2\Delta d^3 + 3dv^2\Delta d^2 + 3d^2v^2\Delta d + d^3v^2 + 2v\Delta d^3\Delta v + 6dv\Delta d^2\Delta v + 6d^2v\Delta d\Delta v \\ + 2d^3v\Delta v + \Delta d^3v^2 + 3d\Delta d^2\Delta v^2 + 3d^2\Delta d\Delta y^2 + d^3\Delta v^2 \end{array}\right)$$

Eliminate Small Terms.

[1] "Simulation of Hypervelocity Impacts" http://hitf.jsc.nasa.gov/hitfpub/simulations/index.html (November 21, 2005)

$$= \frac{\pi\rho}{12}\left(3d^2v^2\Delta d + d^3v^2 + 2d^3v\Delta v\right)$$

Subtract K.E.

$$\Delta K.E. = \frac{\pi\rho}{12}\left(3d^2v^2\Delta d + 2d^3v\Delta v\right)$$

Divide by K.E. Simplify.

$$\frac{\Delta K.E.}{K.E.} = \frac{\left(3v\Delta d + 2d\Delta v\right)}{dv}$$

Let d = 0.4 mm, Δd = .05 mm, v = 6.94 km/s, and Δv = .005 km/s.

$$\frac{\Delta K.E.}{K.E.} = \frac{3(6.94)(0.005) + 2(0.4)(0.005)}{(0.4)(6.94)} = 0.0389 = 3.89\%$$

Relative Uncertainty of Wave Signal Energy

Eraw = Raw Wave Signal, V^2 - μs
Δ*Eraw* = Raw Wave Signal Uncertainty, V^2 - μs
G = Gain, dB
N = resolution, bits
V = Voltage Range, Volts

$$W.S.E. = \frac{Eraw}{\left(10^{\frac{G}{20}}\right)^2}$$

$$W.S.E. + \Delta W.S.E. = \frac{Eraw + \Delta Eraw}{\left(10^{\frac{G}{20}}\right)^2}$$

$$\Delta W.S.E. = \frac{\Delta Eraw}{\left(10^{\frac{G}{20}}\right)^2}$$

$$\Delta Eraw = \frac{V}{2^N}$$

Let V = 1 Volt and N = 10.

$$\Delta Eraw = \frac{1}{2^{10}} = 0.000977 \ \text{V}^2 \text{ - } \mu\text{s}$$

Let $Eraw$ = 0.25 V^2 - μs and $\Delta Eraw$ = 0.000977

$$\frac{\Delta W.S.E.}{W.S.E.} = \frac{\Delta Eraw}{Eraw} = \frac{0.000977}{0.25} = 0.00391 = 0.391\%$$

Target Photographs

Targets A-1 (Figure 11) and A-2 (Figure 12) consisted of a fiberglass front plate followed by an aluminum backplate. Target size was 30" x 30", with 0.25" thick fiberglass and 1/8" thick aluminum. Standoff between the fiberglass and aluminum was 12". The plates were connected using (8) 0.5" all-thread rods. L-shaped angles added to the back of the aluminum plate were used to attach the target to a target support stand, which was placed in the target chamber. The fiberglass panel was a 19 ply (0.90) woven material. Target A-1 contained grommets that isolated the fiberglass panel from the all-thread. Target A-2 was similar to Target A-1 but the fiberglass panel was not isolated from the all-thread (no grommets).

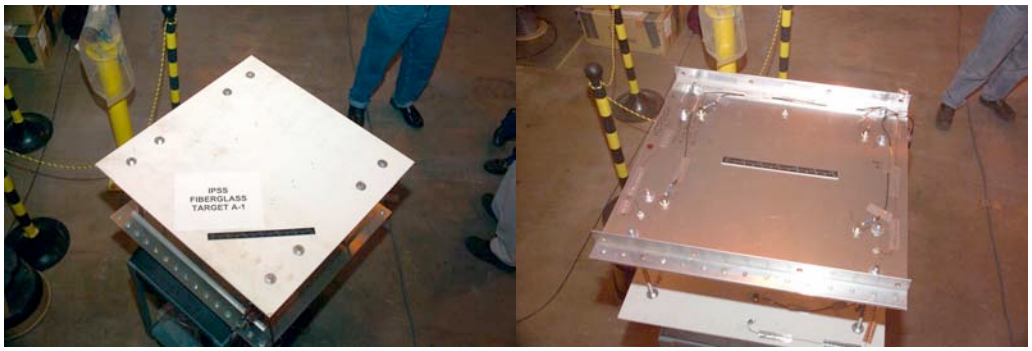

Figure 11: Target A-1. Left: Top View. Right: Bottom View.

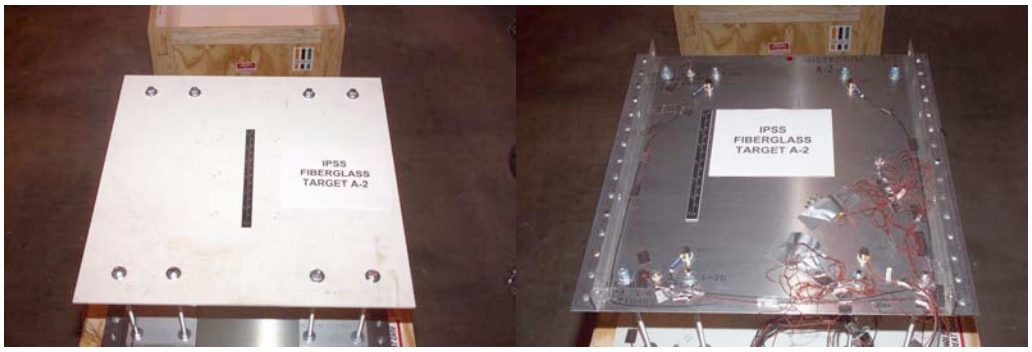

Figure 12: Target A-2 Left: Top View. Right: Bottom View.

Target B-1 (Figure 13) used two fiberglass plates to model MMOD impacts with a trajectory that would go through the WLE panel and not intersect directly with the wing spar. Target B-1 consisted of a 30 x 30 19 ply fiberglass panel, a 12" gap, a second 19 ply fiberglass panel, a 3.8" gap, and a 0.125" thick aluminum plate. Target B-1 contained grommets that isolated the fiberglass panel from the 0.5" all-thread.

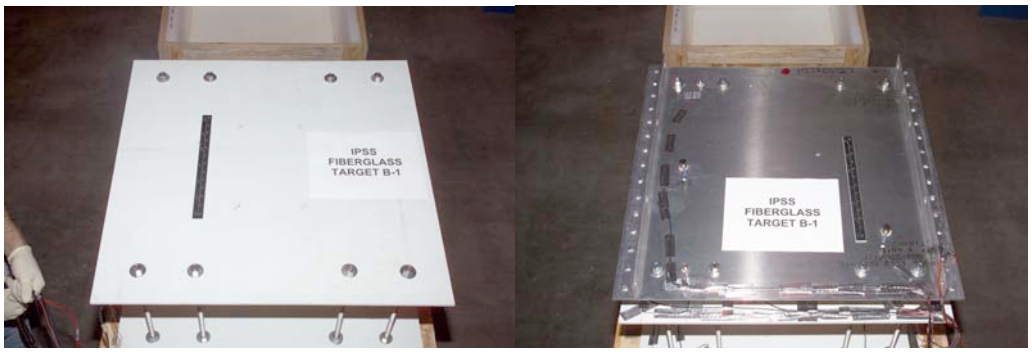

Figure 13: Target B-1. Left: Top View. Right: Bottom View.

Target C-1 (Figure 14) consisted of a 34" x 34" 20-ply fiberglass panel. L-shaped angles added to the back of the fiberglass panel were used to attach the target to a target support stand. Target C-2 was identical to Target C-1

Figure 14: Fiberglass Panel Target C-1. Front View.

Target Fg(RCC)-1 (Figure 15) consisted of a 20-ply fiberglass panel formed to the same dimensions of an actual RCC panel 16R. Target Fg(RCC)-2 was identical to Target Fg(RCC)-1.

Figure 15: Target Fg(RCC)-1

Target RCC16R (Figure 16) was a component part of a Shuttle leading edge made by Boeing. It is made from carbon-carbon, a material that can withstand temperatures in excess of 2300 degrees Fahrenheit encountered on re-entry.

Figure 16: Target RCC16R on Rail System.

Targets A-1, Ag-1, B-1, and Bg-1 (Figure 17 and Figure 18) were 34" x 34" in size, with an array of tile and aluminum skin-stringers substructure. The tiles were manufactured and densified to flight specs, bonded by standard SIP specifications to the aluminum

skin-stringers substrate that was cleaned, primed and prepared per flight specs. Target type A resembled lower wing structure toward the wing aft. The tiles were 6" x 6" x 1.3" thick L1-900 in a 19 tile array, bonded to 0.16" thick SIP and to a 0.063" thick Al 2024T81, with hat shaped stiffeners attached (riveted) to provide reasonable target stiffness. Tiles on some targets were installed without gap fillers (designated "A-1" and "B-1"), while the tiles on other targets were installed with gap fillers (designated "Ag-1" and "Bg-1").

Figure 17: Tile Targets A-1 (Left) and Ag-1 (Right)

Figure 18: Tile Target B-1 (Left) and Bg-1 (Right)

Data Example

The appendix for each target features a data sheets, a snapshot of the waveforms recorded on each sensor, and photos of the actual damage. Shown in figures 17-22 is information for Target Fg(RCC)-2, shot #3.

The data sheets for each shot (Figure 17) give detailed information on the projectile size and velocity, sensor serial numbers and locations, preamp and attenuators used, and any additional comments on the impact.

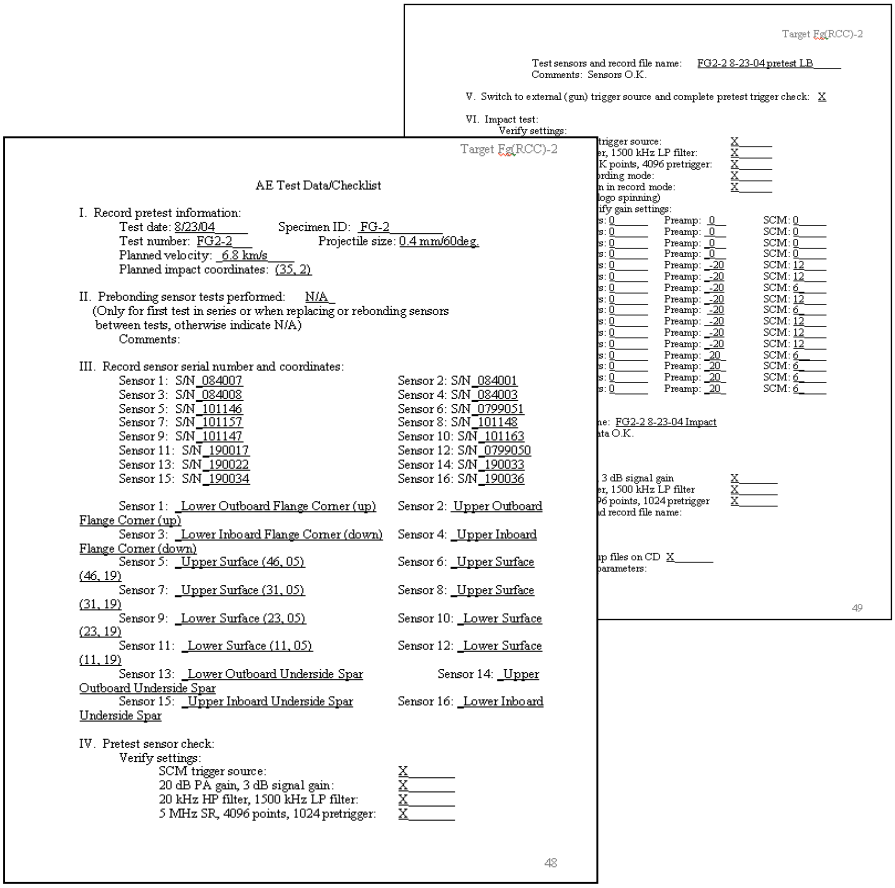

Target Fg(RCC)-2

AE Test Data/Checklist

I. Record pretest information:
Test date: 8/23/04 Specimen ID: FG-2
Test number: FG2-2 Projectile size: 0.4 mm/60deg.
Planned velocity: 6.8 km/s
Planned impact coordinates: (35, 2)

II. Prebonding sensor tests performed: N/A
(Only for first test in series or when replacing or rebonding sensors between tests, otherwise indicate N/A)
Comments:

III. Record sensor serial number and coordinates:

Sensor 1: S/N 084007	Sensor 2: S/N 084001
Sensor 3: S/N 084008	Sensor 4: S/N 084003
Sensor 5: S/N 101146	Sensor 6: S/N 0799051
Sensor 7: S/N 101157	Sensor 8: S/N 101148
Sensor 9: S/N 101147	Sensor 10: S/N 101163
Sensor 11: S/N 190017	Sensor 12: S/N 0799050
Sensor 13: S/N 190022	Sensor 14: S/N 190033
Sensor 15: S/N 190034	Sensor 16: S/N 190036

Sensor 1: Lower Outboard Flange Corner (up) Sensor 2: Upper Outboard Flange Corner (up)
Sensor 3: Lower Inboard Flange Corner (down) Sensor 4: Upper Inboard Flange Corner (down)
Sensor 5: Upper Surface (46, 05) Sensor 6: Upper Surface (46, 19)
Sensor 7: Upper Surface (31, 05) Sensor 8: Upper Surface (31, 19)
Sensor 9: Lower Surface (23, 05) Sensor 10: Lower Surface (23, 19)
Sensor 11: Lower Surface (11, 05) Sensor 12: Lower Surface (11, 19)
Sensor 13: Lower Outboard Underside Spar Sensor 14: Upper Outboard Underside Spar
Sensor 15: Upper Inboard Underside Spar Sensor 16: Lower Inboard Underside Spar

IV. Pretest sensor check:
Verify settings:
SCM trigger source: X
20 dB PA gain, 3 dB signal gain: X
20 kHz HP filter, 1500 kHz LP filter: X
5 MHz SR, 4096 points, 1024 pretrigger: X

48

Target Fg(RCC)-2

Test sensors and record file name: FG2-2 8-23-04 pretest LB
Comments: Sensors O.K.

V. Switch to external (gun) trigger source and complete pretest trigger check: X

VI. Impact test:
Verify settings:
trigger source: X
er, 1500 kHz LP filter: X
K points, 4096 pretrigger: X
rding mode: X
n in record mode: X
logo spinning)
ify gain settings:

s: 0	Preamp: 0	SCM: 0
s: 0	Preamp: 0	SCM: 0
s: 0	Preamp: 0	SCM: 0
s: 0	Preamp: 0	SCM: 0
s: 0	Preamp: -20	SCM: 12
s: 0	Preamp: -20	SCM: 12
s: 0	Preamp: -20	SCM: 6
s: 0	Preamp: -20	SCM: 12
s: 0	Preamp: -20	SCM: 6
s: 0	Preamp: -20	SCM: 12
s: 0	Preamp: -20	SCM: 12
s: 0	Preamp: -20	SCM: 6
s: 0	Preamp: 20	SCM: 6
s: 0	Preamp: 20	SCM: 6
s: 0	Preamp: 20	SCM: 6

ne: FG2-2 8-23-04 Impact
ata O.K.

3 dB signal gain X
er, 1500 kHz LP filter X
96 points, 1024 pretrigger X
d record file name:

p files on CD X
parameters:

49

Figure 19: AE Test Data/Checklist Target Fg(RCC)-2, Shot #3

The impact waveform shows the amplitude and arrival time of the raw wave signal. The units for the x-axis are µs and the units for the y-axis are volts. On this particular shot, sensors 1-4 are located on the flange, sensors 5-8 on the upper surface, sensors 9-12 on the lower surface, and sensors 13-16 on the spar. A photo of the target is shown in Figure 15.

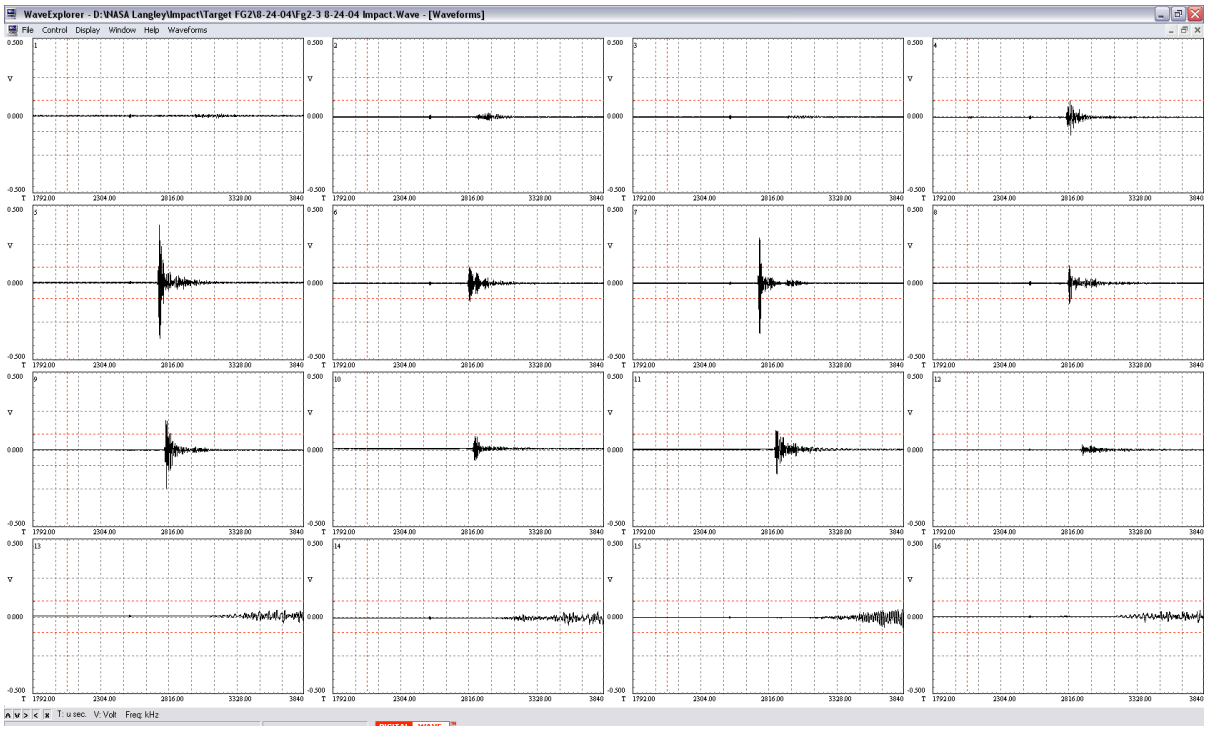

Figure 20: Fg(RCC)-2 Shot #3 Impact Waveform

Notice how each group of sensors have a similar signal. Sensors 5-8, for example, are located very close to the impact location on the surface of the target. These waveforms have sharp peaks which decrease in amplitude quickly. The signal arrives at these sensors before it arrives at the spar sensors (13-16). By the time it reaches the spar sensors, the signal has reflected off many surfaces and is characterized by a smaller signal which gradually increases in amplitude.

A variety of photos were taken after each test. Figure 21 is a photograph from the front side of the target. A ruler is included for scale.

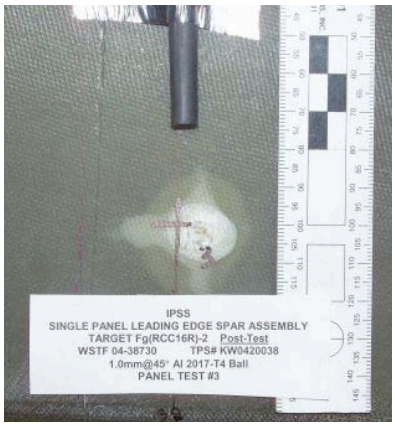

Figure 21: Fg(RCC)-2 Shot #3 Impact Damage

Fiberglass is composed of multiple layers. The delamination area for each layer varied depending upon the impactor speed and angle. The damage to these layers is shown clearly with backlighting (Figure 22).

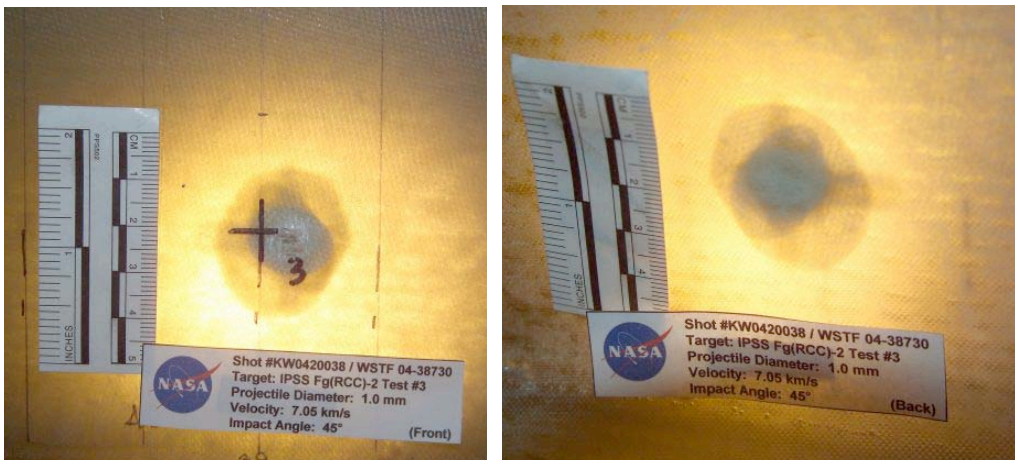

Figure 22: Fg(RCC)-2 Shot #3 Backlit Impact Damage (Left: Front Side, Right: Back Side)

Spalling

Target RCC16R and the multilayer targets (A-1, A-2, and B-1) experienced spalling damage.

For the multilayer targets, after the impactor hit the first layer of fiberglass, small ejecta impacted the second layer of fiberglass (Figure 23). The secondary impacts reflected back up the metal rods that joined the layers together resulting complex data recorded by sensors on the first layer. This process is discussed further in the Target A-1, A-2, and B-1 Report, but it is important to note that spalling damage made these targets unique.

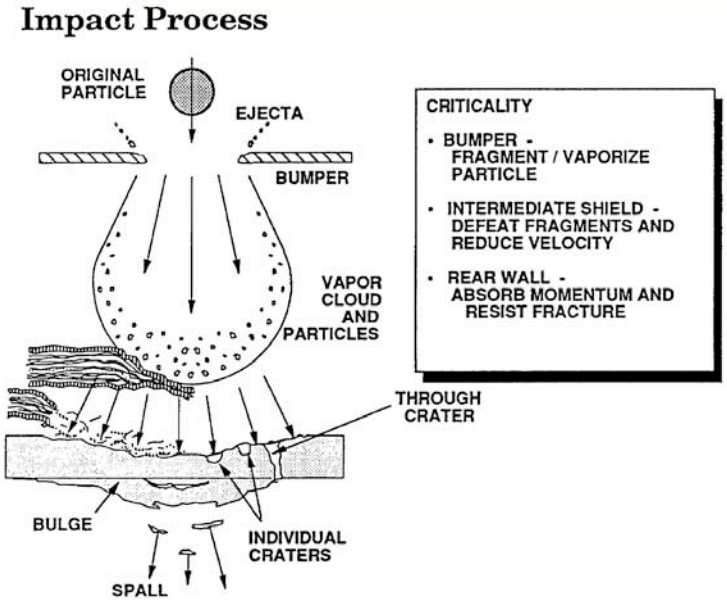

Figure 23: Multilayer Penetration Mechanisms[2]

[2] Figure 3-1 Multi-layer penetration mechanisms. "Structural Damage Prediction and Analysis for Hypervelocity Impacts – Handbook" p. 3-9 N.C. Elfer, 1996

Conclusions

- Ultrasonic Sensors were successfully bonded to all targets with Lord 202 Acrylic Adhesive.

- Ultrasonic Sensors operated well in near-vacuum (6-8 Torr) inside the vacuum chamber at Johnson Space Center's White Sands Testing Facility.[3]

- Impacts created detectable ultrasonic signals at high (>50 kHz) frequencies which should be above flight noise.[4]

- Ultrasonic signals were detected with small, lightweight sensors capable of space flight.[5][6]

- Wave propagation characteristics of the cross-ply fiberglass targets were measured and used in the analysis of the wave signal energy.

- Wave signal energy correlated well with kinetic energy and impact damage.

This test successfully demonstrated the ability for a wing leading edge impact detection system (WLEIDS) to model the kinetic energy response and material damage below, at and above complete penetration of the projectile through the target.

[3] B1025 sensors also functioned well in deep vacuum of ESEM. Michael Horn, NASA LaRC, email 2005.
[4] Based on measurement of noise spectra on F16 bulkhead at full throttle, there will not be significant noise power above 50kHz.
[5] Sensors passed 18,000 g shock test. Henry Whitesel, Naval Surface Warfare Center, verbal communication 1998.
[6] DWC sensors survived intense radiation environment. Dane Spearing, LANL, verbal communication 2003.

REPORT DOCUMENTATION PAGE

Form Approved
OMB No. 0704-0188

1. REPORT DATE *(DD-MM-YYYY)*	2. REPORT TYPE	3. DATES COVERED *(From - To)*
01- 09 - 2007	Contractor Report	

4. TITLE AND SUBTITLE
Hypervelocity Impact (HVI) - Volume 1: General Introduction

5a. CONTRACT NUMBER
NNL05AC19T

5b. GRANT NUMBER

5c. PROGRAM ELEMENT NUMBER

6. AUTHOR(S)
Gorman, Michael R.; and Ziola, Steven M.

5d. PROJECT NUMBER

5e. TASK NUMBER

5f. WORK UNIT NUMBER
377816.06.03.03.06

7. PERFORMING ORGANIZATION NAME(S) AND ADDRESS(ES)
NASA Langley Research Center
Hampton, VA 23681-2199

8. PERFORMING ORGANIZATION REPORT NUMBER

9. SPONSORING/MONITORING AGENCY NAME(S) AND ADDRESS(ES)
National Aeronautics and Space Administration
Washington, DC 20546-0001

10. SPONSOR/MONITOR'S ACRONYM(S)
NASA

11. SPONSOR/MONITOR'S REPORT NUMBER(S)
NASA/CR-2007-214885/Vol1

12. DISTRIBUTION/AVAILABILITY STATEMENT
Unclassified - Unlimited
Subject Category 70
Availability: NASA CASI (301) 621-0390

13. SUPPLEMENTARY NOTES
Langley Technical Monitor: Eric I. Madaras
An electronic version can be found at http://ntrs.nasa.gov

14. ABSTRACT

During 2003 and 2004, the Johnson Space Center's White Sands Testing Facility in Las Cruces, New Mexico conducted hypervelocity impact tests on the space shuttle wing leading edge. Hypervelocity impact tests were conducted to determine if Micro-Meteoroid/Orbital Debris impacts could be reliably detected and located using simple passive ultrasonic methods. This volume contains an executive summary, overview of the method, brief descriptions of all targets, and highlights of results and conclusions.

15. SUBJECT TERMS
Hypervelocity impact tests; Space shuttle; Wing leading edge; Debris; Impact damage

16. SECURITY CLASSIFICATION OF:			17. LIMITATION OF ABSTRACT	18. NUMBER OF PAGES	19a. NAME OF RESPONSIBLE PERSON
a. REPORT	b. ABSTRACT	c. THIS PAGE			STI Help Desk (email: help@sti.nasa.gov)
					19b. TELEPHONE NUMBER *(Include area code)*
U	U	U	UU	33	(301) 621-0390